Semiconductor Physics, Quantum Electronics & Optoelectronics, 2018. V. 21, N 2. P. 180-186.

Optoelectronics

Suitable factorization of the total intersubband scattering rates for efficient calculation of the current densities and gain characteristics in quantum cascade lasers

S.S. Kurlov[1, 2], M.P. Semtsiv[1], Z.Ya. Zhuchenko[2], G.G. Tarasov[2], W.T. Masselink[1]

[1] *Department of Physics, Humboldt-Universität zu Berlin, Newtonstraße 15, 12489 Berlin, Germany*

[2] *V. Lashkaryov Institute of Semiconductor Physics, Nas of Ukraine, 41, prospect Nauky, 03680 Kyiv, Ukraine,*

Abstract. Suitable factorization of the intersubband scattering rates is performed for the temperature dependent electron transport model of mid-infrared quantum cascade lasers (QCL). In this case, the total intersubband scattering rate is presented as a sum of individual processes: longitudinal optical phonon, roughness interface, and acoustic phonon scatterings. The individual scattering rate is reduced to a product of the overlap integral for the squared moduli of the envelope functions and the temperature factor that depends on the transition energy and material. This presentation significantly reduces computational efforts in comparison with the *ab initio* models of full quantum transport in QCL preserving good agreement between the theory and experiment, as well.

Keywords: quantum cascade laser, intersubband scattering rate, current density, gain characteristics.

doi: https://doi.org/10.15407/spqeo21.02.180
PACS 42.55.-f, 42.55.Ah

Manuscript received 02.04.18; revised version received 30.04.18; accepted for publication 27.06.18; published online 03.07.18.

1. Introduction

Quantum cascade lasers (QCLs) firstly invented and demonstrated more than 20 years ago at Bell Laboratories [1] are the semiconductor electrically pumped laser sources that use electron transitions between the subbands in the conduction band of a multiple-quantum-well heterostructure. Injected electron makes a small by energy intersubband transition within the quantum well during its motion between tunnel-coupled quantum wells of multilayer heterostructure emitting light in each cascade. While the position of energy levels within a quantum well is mainly determined by one-dimensional confinement, *i.e.*, by the thickness of the layers, rather than the material, the emission wavelength of QCLs spreads over a wide spectral range of infra-red diapason even in the same material system. Recently, QCLs of the mid infrared (MIR) frequency range demonstrate a record high wallplug efficiency (WPE), high continuous wave (CW) output power, single mode operation, and wide tunability [2]. A WPE value of 53% at 40 K is already reached. Very high peak power close to 190 W has been obtained from a broad area QCL of ridge width 400 μm [2]. Now, QCLs can generate high CW power output up to 5.1 W at room temperature, and cover the spectral range from 3 up to 300 μm by simple varying the material components. Broadband heterogeneous QCLs with the broad spectral range from 3 to 12 μm, wavelength agile QCLs based on monolithic sampled grating design, and on-chip beam QCL combiner are being developed for the next generation tunable mid-infrared source [3, 4]. The far-IR (terahertz) QCLs are now presented by a new class of light sources with room temperature operation in the terahertz (THz) spectral range, with nearly 2 mW of optical power and significant tunability [5-7]. These developments open up the terahertz region of the spectrum for a wide range of applications in biological imaging, medical imaging, security, spectroscopy, and communications [8-11].

However, further development of new QCL sources and optimization of their operation needs also adequate theoretical maintenance. Recently, theoretical models based on Monte Carlo simulations [12], on non-equilibrium Green functions [13, 14] are widely used for calculation of carrier transport and prediction of intersub-band gain. As a rule, these models require substantially large computational efforts. An alternative approach combines a one-dimensional system of rate equations with the three-dimensional calculation of intersubband scattering times [15], thus significantly reducing the numerical time. Beside the computing time limitation, it has to be taken into account that QCLs are based on multiple-quantum-well heterostructures with complex subband structure needed to supply sufficient gain for lasing. Calculation of this structure has to be performed including its bias dependence and location of charge as well as the non-parabolicity of the band structure,

scattering effects, and the optical mode confinement. Also, the substantial scattering of the values of parameters such as the layer thicknesses, composition fluctuations, interfaces, unavoidable for multiple-quantum-well heterostructures influence the lasing properties of QCLs. Therefore, sufficiently compact and straightforward models are necessary, in particular for design purposes and QCL optimization for a given wavelength, which, at the same time, predict the gain maximum as well as current densities with reasonable accuracy. Recently, such compact model for the efficient simulation of the gain characteristics in THz QCLs based on the self-consistent solution of the Schrödinger and Poisson equations in the framework of a one-dimensional scattering-rate approach has been developed [16]. In this model, the total intersubband scattering rates were factorized into the squared modulus of the respective dipole matrix elements and an energy-dependent factor, which were used as an approximation for the various scattering processes. It has been shown that the model allows the efficient calculation of the gain characteristics and current densities due to a substantial reduction of numerical effort in case of various THz QCLs based on either the bound-to-continuum design or the resonant-longitudinal-optical-phonon design. Further, this model has been extended to MIR QCLs by including the energy dependence of the intersubband scattering rates for the energies higher than the longitudinal optical phonon energy [17]. This energy dependence was obtained from a phenomenological fit of the intersubband scattering rates based on published lifetimes of a number of MIR QCLs. In the developed model, the total intersubband scattering rate was written as the product of the overlap integral for the squared moduli of the envelope functions and a phenomenological factor that depended only on the transition energy. The model was successfully applied to calculation of low-temperature current-voltage, power-current, and energy-photon flux characteristics for a QCL emitting at 5.2 μm. In view of successful application of our phenomenological scattering-rate model [17] for low-temperature MIR QCLs, in this paper we perform factorization of individual intersubband scattering rates which are longitudinal optical phonon, roughness interface, and acoustic phonon scatterings entering the total intersubband scattering rate, thus extending the model for a wide temperature range. This factorization is a peculiar mathematical procedure that can be further applied for efficient calculation of the current densities and gain characteristics in quantum cascade lasers even for room temperature.

2. Rate equations approach

Following [18], the rate equations that describe the electron dynamics in QCLs can be written as

$$\frac{dn_i^s}{dt} = \sum_{j\neq i}\left(R_{ji}n_j^s - R_{ij}n_i^s\right) + \sum_{j\neq i}\left(W_{ji}^{st}n_j^s - W_{ij}^{st}n_i^s\right). \qquad (1)$$

Here, n_i^s is the electron sheet density of subband i which arises due to energy quantization in one dimensional quantum well whereas the in-plane electron motion is free. R_{ij} stand for the rates of relaxation transitions caused by scattering due to interaction of electrons with phonons, electrons, impurities, and defects in the semiconductor heterostructures. W_{ij}^{st} denotes the rates of the stimulated optical transitions between the E_i and E_j energy levels which are in resonance with the frequency of optical field $\omega = \omega_{ij} = \left|E_i - E_j\right|/\hbar$ and are proportional to the optical intensities in the corresponding lasing modes [19]. While the QCL is typically modeled as a biased periodic heterostructure the simulation can be restricted to a single representative period far away from the contacts, complemented by the periodic boundary conditions [15]. In this case, the effects like the fabrication tolerance, local fluctuations of the light intensity, domain formation [20], *etc*. are excluded. For a representative period indexes i, j in Eq. (1) run over 1, .., N, where N is the number of subbands in each period, and $R_{i,j}$, W_{ij}^{st} include the transitions to all equivalent levels in the different periods. The intersubband scattering rates $R_{i,j}$ can be self-consistently determined using the corresponding Hamiltonian [21, 22]. This approach is based on well known material parameters such as the effective mass. It can be considered as a compromise between needed accuracy, on the one hand, and relative numerical efficiency, on the other hand, for simulation of QCLs.

2.1. Factorization of the scattering rate caused by LO phonons

In case of lightly doped semiconductors used in QCLs, we have $\left(E_{ik} - E_i^{\mathrm{F}}\right) >> k_{\mathrm{B}}T_e$ and the Fermi–Dirac distribution approaches a classical Maxwell–Boltzmann distribution $f_{\mathrm{MB}}(k) = \hbar^2 \exp\left(-\hbar^2k^2/2m^*k_{\mathrm{B}}T_e\right)/m^*k_{\mathrm{B}}T_e$, where k_{B}, m^*, and T_e are the Boltzmann constant, effective mass and temperature for electrons, respectively.

The transition rate R_{ij}^s for a particular intersubband scattering mechanism s in QCLs can be written as in [22]:

$$R_{ij}^s = \int_0^\infty dk\, k\, R_{ij}^s(k) f_{\mathrm{MB}}(k)\ . \qquad (2.1.1)$$

Here, $R_{ij}^s(k)$ is the total transition rate of electron from a state with momentum k in the initial i-th subband to the states in the j-th subband.

For scattering by longitudinal optical phonons, the function $R_{ij}^s(k)$ has the form [21]:

$$R_{ij}^{LO}(k) = \alpha_{LO}\int_0^\infty dK_z F_{ij}^1(k, K_z)\left|G_{ij}(K_z)\right|^2, \qquad (2.1.2)$$

where

$$F_{ij}^1(k, K_z) = \Theta\left(k^2 + \frac{2m^*\Delta_{ij}^{LO}}{\hbar^2}\right)\times$$

$$\times\left[K_z^4+2K_z^2\left(2k^2+\frac{2m^*\Delta_{ij}^{LO}}{\hbar^2}\right)+\left(\frac{2m^*\Delta_{ij}^{LO}}{\hbar^2}\right)^2\right]^{-1/2},$$

and the form factor for phonon wavevector K_z is defined as

$$G_{ij}(K_z)=\int_{-\infty}^{\infty}dz\psi_j^*(z)\,e(-iK_z z)\psi_i(z).$$

$\alpha_{LO}=\dfrac{m^*e^2\omega_{LO}}{2\pi\hbar^2}\left(\varepsilon_\infty^{-1}-\varepsilon_s^{-1}\right)\left(N_{LO}+\dfrac{1}{2}\pm\dfrac{1}{2}\right)$, Θ is the Heaviside step function, and $\Delta_{ij}^{LO}=E_i-E_j\mp E_{LO}$.

The LO phonon branch $E_{LO}(\omega)$ is considered as dispersionless, $E_{LO}(\omega)=E_{LO}\cong\hbar\omega_{LO}$, ε_∞ and ε_s are the high- and low-frequency permittivities of the semiconductor, respectively;

$N_{LO}=\left[\exp(\hbar\omega_{LO}/k_BT_l)-1\right]^{-1}$

is the LO phonon occupation number in the emission (sign "+") and absorption (sign "–") processes, T_l is lattice temperature.

Inserting Eq. (2.1.2) into Eq. (2.1.1), one gets

$$R_{ij}^{LO}=\alpha_{LO}\int_{-\infty}^{\infty}dK_z\left|G_{ij}(K_z)\right|^2\left(\int_0^{\infty}dkkF_{ij}^1(k,K_z)f_{MB}(k)\right)=$$

$$=\alpha_{LO}\int_{-\infty}^{\infty}dK_z\left|G_{ij}(K_z)\right|^2Q_{ij}(K_z),\qquad(2.1.3)$$

where

$$Q_{ij}(K_z)=\int_0^{\infty}dkkF_{ij}^1(k,K_z)f_{MB}(k).\qquad(2.1.4)$$

After integration over k in Eq. (2.1.4), the function $Q_{ij}(K_z)$ turns to:

$$Q_{ij}(K_z)=\frac{\sqrt{\pi\mu}}{2K_z}\exp(a)\operatorname{erfc}\left(\sqrt{a}\right),\ \text{if}\ \Delta_{ij}^{LO}\ge0,\qquad(2.1.5a)$$

with $\mu=\hbar^2/2m^*k_BT_l$, $b=2m^*\Delta_{ij}^{LO}/\hbar^2$, and $a=\mu\left(\left(K_z^2+b\right)/2K_z\right)^2$ or

$$Q_{ij}(K_z)=\frac{\sqrt{\pi\mu}}{2K_z}\exp(a)\operatorname{erfc}\left(\sqrt{a-\mu b}\right),\ \text{if}\ \Delta_{ij}^{LO}<0.\qquad(2.1.5b)$$

The complementary error function erfc(x) has an asymptotic representation for a large value of x [23]:

$$\operatorname{erfc}(x)\approx\frac{e^{-x^2}}{x\sqrt{\pi}}\sum_{k=0}^{\infty}\frac{(-1)^k(2k-1)!!}{\left(2x^2\right)^k}.\qquad(2.1.6)$$

The asymptotic series in Eq. (2.1.6) is not convergent, however, for large x the function erfc(x) can be substantially well approximated already by a few first terms of the series, say,

$$\operatorname{erfc}(x)\approx\frac{e^{-x^2}}{x\sqrt{\pi}}\left(1-\frac{1}{\left(2x^2\right)}\right).\qquad(2.1.7)$$

Taking this into account, we find that in the case of large value of K_z, when $K_z^2>>|b|$ and $a\to\mu K_z^2/4$,

$$Q_{ij}(K_z)\to\frac{1}{K_z^2}.\qquad(2.1.8)$$

Thus, the integrand in Eq. (2.1.3) is a product of two rapidly decaying functions $\left|G_{ij}(K_z)\right|^2$ and $Q_{ij}(K_z)$, if $K_z\to\infty$. Turning back to calculation of transition rate R_{ij}^{LO}, let's split the interval of integration into two parts:

$$R_{ij}^{LO}=2\alpha_{LO}\lim_{K_z^{\lim}\to\infty}\left[\begin{array}{l}\int_0^{K_z^{\lim}}dK_z\left|G_{ij}(K_z)\right|^2Q_{ij}(K_z)+\\ \int_{K_z^{\lim}}^{\infty}dK_z\left|G_{ij}(K_z)\right|^2Q_{ij}(K_z)\end{array}\right].\qquad(2.1.9)$$

The second term in Eq. (2.1.9) tends to zero, whereas for calculation of the first term we apply the first mean value theorem for definite integrals. While the function $Q_{ij}(K_z)$ is continuous on the interval $\left[0,K_z^{\lim}\right]$, and the function $\left|G_{ij}(K_z)\right|^2$ is an integrable function that does not change its sign on the same interval, then there exists the point $\overline{K}_z$ in the interval $\left[0,K_z^{\lim}\right]$ such that

$$R_{ij}^{LO}=2\alpha_{LO}\lim_{K_z^{\lim}\to\infty}\left[\int_0^{K_z^{\lim}}dK_z\left|G_{ij}(K_z)\right|^2Q_{ij}(K_z)\right]=$$

$$=2\alpha_{LO}\lim_{K_z^{\lim}\to\infty}Q_{ij}\left(\overline{K}_z\right)\int_0^{K_z^{\lim}}dK_z\left|G_{ij}(K_z)\right|^2.\qquad(2.1.10)$$

For the large value of $K_z^{\lim}$, $\overline{K}_z\to\text{const}$ and Eq. (2.1.10) takes the form

$$R_{ij}^{LO}=2\alpha_{LO}\lim_{K_z^{\lim}\to\infty}Q_{ij}\left(\overline{K}_z\right)\int_0^{K_z^{\lim}}dK_z\left|G_{ij}(K_z)\right|^2=$$

$$=2\alpha_{LO}Q_{ij}\left(\overline{K}_{\lim}\right)\int_0^{\infty}dK_z\left|G_{ij}(K_z)\right|^2.\qquad(2.1.11)$$

This equation can be rewritten in terms of integral of overlapping for the electron wavefunctions, ζ_{ij}:

$$R_{ij}^{LO}=2\alpha_{LO}Q_{ij}\left(\overline{K}_{\lim}\right)\int_0^{\infty}dK_z\left|G_{ij}(K_z)\right|^2=$$

$$=2\alpha_{LO}Q_{ij}\pi\int_{-\infty}^{\infty}\left|\psi_j(z)\right|^2\left|\psi_i(z)\right|^2dz=2\alpha_{LO}Q_{ij}\pi\zeta_{ij}.\qquad(2.1.12)$$

2.2. Factorization of the scattering rates caused by acoustic phonons

To calculate the acoustic phonon scattering rate, we take into account that the energies of acoustic phonons ω_A are as usual significantly lower than the typical intersubband separations $\Delta E_{ij}=E_j-E_i$ which can be of several hundred meV by their value. Besides, the acoustic phonon branch can be approximated by a linear function of phonon wave vector module K, $\omega_A=\upsilon_SK$, where υ_S

is a velocity of a sound wave. In this case, the transition rate R_{ij}^A for acoustic phonon scattering can be written in accord with Eq. (2.1.1) as

$$R_{ij}^A = \int_0^\infty dk\, k R_{ij}^A(k) f_{\mathrm{MB}}(k) \,. \tag{2.2.1}$$

Here, $R_{ij}^A(k)$ defines the rate for electron from a state with the momentum k in the initial i-th subband to transit into all states in the j-th subband with participation of acoustic phonons. Following Ref. [21], the function $R_{ij}^A(k)$ can be calculated using the expression:

$$R_{ij}^A(k) = \frac{D_A^2}{2\rho_c \upsilon_S (2\pi)^2} \times$$
$$\times \iiint \left(N_A + \frac{1}{2} \pm \frac{1}{2} \right) K \delta\left(E_{jk_j} - E_{ik_i} \mp \hbar\omega_A \right) dK_z d\vec{K}_{xy} \,, \tag{2.2.2}$$

where D_A is an acoustic deformation potential, ρ_c is the crystal density, N_A is a phonon occupation number of a mode with the wave vector $\vec{K}$:

$$N_A = \left[\exp\left(\frac{\hbar\omega_A}{k_{\mathrm{B}} T_l} \right) - 1 \right]^{-1} . \tag{2.2.3}$$

$\vec{K}_{xy}$ and K_z are in-plane and perpendicular components of phonon wave vector;

$$E_{ik_i} = E_i + \frac{\hbar^2 k_i^2}{2m^*} \text{ and } E_{jk_j} = E_j + \frac{\hbar^2 k_j^2}{2m^*} .$$

Let us take into account that for all but the lowest temperatures Eq. (2.2.3) can be approximated with [22]

$$N_A \approx N_A + 1 \approx \frac{k_{\mathrm{B}} T_l}{\hbar \upsilon_S K} , \tag{2.2.4}$$

and that due to inequality $\hbar\omega_A << \Delta E_{ij}$ the phonon energy can be put zero in Eq. (2.2.2) (the quasi-elastic approximation). In this case, introducing the polar coordinates for the in-plane phonon vector $\vec{K}_{xy}$, Eq. (2.2.2) can be reduced to the form as follows:

$$R_{ij}^A(k) = \frac{k_{\mathrm{B}} T_l m^* D_A^2}{\rho_c \upsilon_S^2 (2\pi)^2 \hbar^3} \times$$
$$\times \iiint_0^{2\pi} \left| G_{ij}(K_z) \right|^2 \delta \left(\begin{matrix} K_{xy}^2 + 2k_i K_{xy} \cos\varphi + \\ + \dfrac{2m^* \Delta E_{ij}}{\hbar^2} \end{matrix} \right) K_{xy}\, dK_{xy}\, d\varphi\, dK_z \,. \tag{2.2.5}$$

Performing integration over K_z and K_{xy} in Eq. (2.2.5), one gets:

$$R_{ij}^A(k) = \alpha_A 2\pi\zeta_{ij} \int_0^{2\pi} \frac{\left(\Theta(\nu_1)\nu_1 + \Theta(\nu_2)\nu_2 \right)}{\nu_1 - \nu_2} d\varphi \tag{2.2.6}$$

with

$$\nu_{1,2} = -k\cos\varphi \pm \sqrt{ (k\cos\varphi)^2 - \frac{2m^* \Delta E_{ij}}{\hbar^2} } \text{ and}$$

$$\alpha_A = \frac{k_{\mathrm{B}} T_l m^* D_A^2}{\rho \upsilon_S^2 (2\pi)^2 \hbar^3} . \tag{2.2.7}$$

As can be seen due to step functions, ν_1 and ν_2 in the numerator of Eq. (2.2.6) have to be positive and $\nu_1 > \nu_2$. If $\Delta E < 0$, $\nu_2 < 0$ and Eq. (2.2.6) reduces to

$$R_{ij}^A(k) = \alpha_A 2\pi\zeta_{ij} \int_0^{2\pi} \left[\frac{-k\cos\varphi + \sqrt{ (k\cos\varphi)^2 - \dfrac{2m^* \Delta E_{ij}}{\hbar^2} }}{2\sqrt{ (k\cos\varphi)^2 - \dfrac{2m^* \Delta E_{ij}}{\hbar^2} }} d\varphi \right] =$$
$$= \alpha_A 2\pi\zeta_{ij} \int_0^{2\pi} \left[\frac{-k\cos\varphi}{2\sqrt{ (k\cos\varphi)^2 - \dfrac{2m^* \Delta E_{ij}}{\hbar^2} }} + \frac{1}{2} \right] d\varphi = \alpha_A 2\pi^2 \zeta_{ij} . \tag{2.2.8}$$

If $\Delta E > 0$, ν_1 and ν_2 can be positive only in the case of $\cos\varphi < 0$ and $R_{ij}^A(k)$ takes the form

$$R_{ij}^A(k) = \alpha_A 2\pi\zeta_{ij} \int_{\pi/2}^{3\pi/2} \frac{(\nu_1 + \nu_2)}{\nu_1 - \nu_2} d\varphi \Rightarrow R_{ij}^A(k) =$$
$$= \alpha_A 2\pi\zeta_{ij} \int_{\pi/2}^{3\pi/2} \left[\frac{-k\cos\varphi}{\sqrt{ (k\cos\varphi)^2 - \dfrac{2m^* \Delta E_{ij}}{\hbar^2} }} d\varphi \right] . \tag{2.2.9}$$

Introducing new variable $y = \sin\varphi$, the integrand can be presented in the following form:

$$R_{ij}^A(k) = \alpha_A 2\pi\zeta_{ij} \int_{-1}^{1} \frac{dy}{\sqrt{a - y^2}} = \alpha_A 2\pi\zeta_{ij} \int_{-\sqrt{a}}^{\sqrt{a}} \frac{dy}{\sqrt{a - y^2}} =$$
$$= \alpha_A 2\pi\zeta_{ij} \arcsin \frac{y}{\sqrt{a}} \Big|_{-\sqrt{a}}^{\sqrt{a}} = 2\alpha_A \pi\zeta_{ij}\pi \,. \tag{2.2.10}$$

with $a = \left(1 - \dfrac{2m^* \Delta E_{ij}}{\hbar^2 k^2} \right)$.

It follows from Eq. (2.2.8) and (2.2.10) that $R_{ij}^A(k)$ is zero if $E_j > E_{ik}$ in the quasi-elastic approximation and $R_{ij}^A(k) = 2\alpha_A \pi^2 \zeta_{ij}$ otherwise. Inserting these results in Eq. (2.2.1) and integrating over k, we get:

$$R_{ij}^A = R_{ij}^A(k) , \tag{2.2.11}$$

that coincides with the results by Jirauschek *et al.* [22], if both emission and absorption will be included by an additional factor of 2.

2.3. Factorization of the scattering rates caused by interface roughness

In the mid-IR QCLs, the main origin of broadening is interface roughness, and it is well known that different transitions see different broadenings [24]. Interface roughness scattering (ifr) is caused by imperfections at

the interface between the barrier and well material in the heterostructure, resulting in a local deviation of the interface $\Delta(x, y)$ from its average position. Normally the interface roughness is characterized by its standard deviation Δ and the correlation length Λ. Following Refs. [22, 24], the total transition rate from an initial state E_{ik} to all states of E_j is defined by the expressions:

$$R_{ij}^{ifr}(k) = \frac{m^*}{\hbar^3}\Delta^2\Lambda^2 V_0^2 \times$$

$$\times \sum_n \left|\psi_i(z_n)\cdot\psi_j^*(z_n)\right|^2 \int_0^\pi d\varphi \exp\left[-\Lambda^2 q^2(\varphi)/4\right]\Theta(q(\varphi)) =$$

$$= \alpha_{ifr}\,\zeta_{ij}\int_0^\pi d\varphi \exp\left[-\Lambda^2 q^2(\varphi)/4\right]\Theta(q(\varphi)) \qquad (2.3.1)$$

with $q^2(\varphi) = 2k^2 + q_0^2 - 2k\sqrt{k^2+q_0^2}\cos\varphi$, $q_0^2 = 2m^*\left(E_i - E_j\right)/\hbar^2$, $\alpha_{ifr} = \frac{m^*}{\hbar^3}\Delta^2\Lambda^2 V_0^2$, and $\zeta_{ij} = \sum_n \left|\psi_i(z_n)\psi_j^*(z_n)\right|^2$. Here, V_0 is the average band offset, and the sum is taken over all the interfaces located at the positions z_n. In the case $E_i > E_j$, $q^2(\varphi) > 0$ for all values of k and φ, whereas if $E_j > E_i$, $q^2(\varphi)$ is real only for all $k^2 > \left|q_0^2\right|$ and for all φ values. Under these conditions, integration over [0, π] by φ can be performed in Eq. (2.3.1), which leads to

$$R_{ij}^{ifr}(k) = \alpha_{ifr}\zeta_{ij}\pi\exp\left[-\frac{\Lambda^2}{4}\left(2k^2+q_0^2\right)\right] I_0\left(\frac{\Lambda^2}{2}k\sqrt{k^2+q_0^2}\right), \qquad (2.3.2)$$

where $I_0(x)$ is the modified Bessel function of the first kind [23].

Inserting Eq. (2.3.2) into Eq. (2.1.1), the total rate for interface roughness scattering takes the form:

$$R_{ij}^{ifr} = \frac{\pi\hbar^2}{m^* k_B T_e}\alpha_{ifr}\zeta_{ij} \times$$

$$\times \int_0^\infty k\,dk \exp\left[\frac{-\hbar^2k^2}{2m^*k_BT_e} - \frac{\Lambda^2}{4}\left(2k^2+q_0^2\right)\right] I_0\left(\frac{\Lambda^2}{2}k\sqrt{k^2+q_0^2}\right). \qquad (2.3.3)$$

To integrate Eq. (2.3.3) over all the interval [0,+∞), one has to take into account the asymptotical behavior of the function $I_0(x)$ [23]:

$$I_0(x) = \frac{\exp(x)}{\sqrt{2\pi x}}\left[1 + O\left(\frac{1}{x}\right)\right] \quad \text{at} \quad x \to \infty \quad \text{and}$$

$$I_0(x) = \sum_{k=0}^{\infty}\frac{\left(x^2/4\right)^k}{(k!)^2} \text{ at } x \to 0. \qquad (2.3.4)$$

According to Eq. (2.3.4), the function $I_0(x)$ equals 1 for $x = 0$ and rapidly grows under x value increase staying all time positive. Nevertheless, the integrand in Eq. (2.3.3), taking into account Eq. (2.3.4) for large value of argument, can be reduced to

$$F_2 = \exp\left[\frac{-\hbar^2k^2}{2m^*k_BT_e} - \frac{\Lambda^2}{4}\left(2k^2+q_0^2\right)\right] I_0\left(\frac{\Lambda^2}{2}k\sqrt{k^2+q_0^2}\right) \approx$$

$$\approx \exp\left[\frac{-\hbar^2k^2}{2m^*k_BT_e} - \frac{\Lambda^2}{4}\left(2k^2+q_0^2\right)\frac{\Lambda^2}{2}k\sqrt{k^2+q_0^2}\right] \Big/ \frac{\Lambda^2}{2}k\sqrt{k^2+q_0^2}$$

and further, if $k^2 >> q_0^2$, to

$$F_2 = \frac{1}{\sqrt{\pi\Lambda^2k^2}}\exp\left[\frac{-\hbar^2k^2}{2m^*k_BT_e}\right]. \qquad (2.3.5)$$

Thus, the integral in Eq. (2.3.3) is convergent under integration over all the interval $[0,\infty)$. Analytically, Eq. (2.3.3) can be solved in the case of $k^2 < q_0^2$. Taking $k\sqrt{k^2+q_0^2} \approx kq_0$ in the argument of the Bessel function, one gets:

$$R_{ij}^{ifr} = \frac{\pi\hbar^2}{m^*k_BT_e}\alpha_{ifr}\zeta_{ij} \times$$

$$\times \int_0^\infty kdk \exp\left[\frac{-\hbar^2k^2}{2m^*k_BT_e} - \frac{\Lambda^2}{4}\left(2k^2+q_0^2\right)\right] I_0\left(\frac{\Lambda^2}{2}kq_0\right) =$$

$$= \frac{\pi\hbar^2}{m^*k_BT_e}\alpha_{ifr}\zeta_{ij}\exp\left(-\frac{\Lambda^2q_0^2}{4}\right) \times$$

$$\times \int_0^\infty kdk \exp\left[\frac{-\hbar^2k^2}{2m^*k_BT_e} - \frac{\Lambda^2}{2}k^2\right] I_0\left(\frac{\Lambda^2}{2}kq_0\right). \qquad (2.3.6)$$

The integral in Eq. (2.3.6) belongs to the following type:

$$R_n = \int_0^\infty z^{2n-1}\exp\left(-az^2\right) I_0(bz)dz = \Gamma(n)\left(2a^n\right)^{-1} L_{-n}\left(b^2/4a\right),$$

where a, b, $n > 0$ and L is the Laguerre polynomial. For $2n-1=1$, one has

$$R_1 = \int_0^\infty z\exp\left(-az^2\right) I_0(bz) = \frac{1}{2a}\exp\left(b^2/4a\right). \qquad (2.3.7)$$

Applying Eq. (2.3.7) to Eq. (2.3.8), one can derive:

$$R_{ij}^{ifr} = \frac{\pi\hbar^2}{m^*k_BT_l}\alpha_{ifr}\zeta_{ij}\left(\frac{\hbar^2}{m^*k_BT_e} + \Lambda^2\right) \times$$

$$\times \exp\left(-\frac{\Lambda^2q_0^2}{4} + \left(\frac{\Lambda^2}{2}q_0\right)^2 \Big/ \left(\frac{2\hbar^2}{m^*k_BT_e} + 2\Lambda^2\right)\right). \qquad (2.3.8)$$

The problem is that in Eq. (2.3.6) the upper limit of integration tends ∞. It means that the condition $k^2 < q_0^2$ inevitably becomes broken for large values of the wave vector k. Nevertheless, it occurs that the integrand in Eq. (2.3.6) differs noticeably from zero only within the interval (0, k_0), where an effective value of k_0 meets the condition $k_0^2 < q_0^2$ for practically the most important interval of ΔE_{ij} meanings from 100 up to 500 meV. While integration from k_0 to ∞ does not contribute to the total value of definite integral in Eq. (2.3.6), integration can be formally extended from 0 to ∞.

By analogy in case of small x values in Eq. (2.3.4), Eq. (2.3.3) will be written as

$$R_{ij}^{ifr} = \frac{\pi\hbar^2}{m^* k_B T_e}\alpha_{ifr}\zeta_{ij}\exp\left(-\frac{\Lambda^2 q_0^2}{4}\right)\times$$
$$\times\int_0^\infty kdk\exp\left[\frac{-\hbar^2 k^2}{2m^* k_B T_e}-\frac{\Lambda^2}{2}k^2\right]\times$$
$$\times\sum_{k=0}^{\infty}\frac{1}{(k!)^2}\left(\left(\frac{\Lambda^2}{2}k\sqrt{k^2+q_0^2}\right)^2\Big/4\right)^k. \quad (2.3.9)$$

If $x < 1$, it is enough to retain only the terms with $k \le 2$ in sum of Eq. (2.3.9) for a very good approximation to the $I_0(x)$ function. As a result the integration in Eq. (2.3.9) reduces to calculations of the integrals like

$$\int_0^\infty y^n\exp(-\mu y)dy = n!\mu^{-n-1}, \text{ where } \mu > 0. \quad (2.3.10)$$

Using Eq. (2.3.10), R_{ij}^{ifr} in Eq. (2.3.9) can be presented in the explicit form

$$R_{ij}^{ifr} = \frac{\pi\hbar^2\alpha_{ifr}\zeta_{ij}}{2m^* k_B T_e\beta}\exp\left(-\tilde{\Lambda}^2 q_0^2\right)\times$$
$$\times\left[1+\frac{1}{\beta}\tilde{\Lambda}^4 q_0^2+\frac{\tilde{\Lambda}^4}{2\beta^2}\left(1+\frac{1}{4}\tilde{\Lambda}^4 q_0^4\right)+\frac{1}{12\beta^3}\tilde{\Lambda}^8 q_0^2+\frac{1}{96\beta^4}\tilde{\Lambda}^8\right] \quad (2.3.11)$$

with $\beta = \hbar^2\left(2m^* k_B T_e\right)^{-1} + \Lambda^2/2$ and $\tilde{\Lambda} = \Lambda/2$.

In the case when $E_j > E_i$, integration in Eq. (2.3.3) has to be performed from $|q_0|$ to ∞. That leads to zero contribution following the arguments given above.

3. Conclusions

Suitable factorization of the intersubband scattering rates has been performed for the temperature dependent electron transport model of mid-infrared quantum cascade lasers. In this case, the total intersubband scattering rate is presented as a sum of individual processes: longitudinal optical phonon, roughness interface, and acoustic phonon scatterings. The individual scattering rate is reduced to a product of the overlap integral for the squared moduli of the envelope functions and the temperature factor that depends on the transition energy and material. In this case, the rate equations written for electron in the state (i, k)

$$\frac{dn_{i,k}}{dt} = \sum_{k'}\left\{\sum_j n_{jk'}R_{jk',ik} - n_{ik}\sum_j R_{ik,jk'}\right\} \quad (3.1)$$

reduces to the form

$$\frac{dn_i}{dt} = \sum_j \varsigma_{ji}\left[n_j\rho_{ji}\left(E_{ji}\right) - n_i\rho_{ij}\left(E_{ij}\right)\right], \quad (3.2)$$

where integration over wave vector $\vec{k}$ is already performed analytically. This presentation significantly reduces computational efforts in comparison with the *ab initio* models of full quantum transport in QCL preserving also good agreement between theory and experiment.

References

1. Faist J., Capasso F., Sivco D.L., Hutchinson A.L., and Cho A.Y. Quantum cascade laser. *Science.* 1994. **264**(5158). P. 553–556.
2. Razeghi M., Bandyopadhyay N., Bai Y., Lu Q., and Slivken S. Recent advances in mid infrared (3-5 μm) Quantum Cascade Lasers. *Opt. Mater. Exp.* 2013. **3**, No 11. P. 1872–1884.
3. Razeghi M., Lu Q.Y., Bandyopadhyay N., Zhou W., Heydari D., Bai Y., and Slivken S. Quantum cascade lasers: from tool to product. *Opt. Exp.* 2015. **23**, No 7. P. 8462–8475.
4. Baranov A.N., Bahriz M., and Teissier R. Room temperature continuous wave operation of InAs-based quantum cascade lasers at 15 μm. *Opt. Exp.* 2016. **24**, No 16. P. 18799–18806.
5. Belkin M.A. and Capasso F. New frontiers in quantum cascade lasers: high performance room temperature terahertz sources. *Phys. Scr.* 2015. **90**. P. 118002–118012.
6. Kindness S.J., Jessop D.S., Wei B., Wallis R., Kamboj V.S., Xiao L., Ren Y., Braeuninger-Weimer P., Aria A.I., Hofmann S., Beere H.E., Ritchie D.A., Degl'Innocenti R. External amplitude and frequency modulation of a terahertz quantum cascade laser using metamaterial/graphene devices. *Sci. Repts*. 2017. **7**, No 1. P. 7657.
7. Liang G., Liu T., Wang Q.J., Recent developments of terahertz quantum cascade lasers. *IEEE Journal of Selected Topics in Quantum Electronics*. 2017. **23**, No 4. P. 1200118.
8. Wei S., Kulkarni P., Ashley K. and Zheng L. Measurement of crystalline silica aerosol using quantum cascade laser–based infrared spectroscopy. *Sci. Repts*. 2017. **7**. P. 13860.
9. Kazakov D., Piccardo M., Wang Y., Chevalier P., Mansuripur T.S., Xie F., Zah C., Lascola K., Belyanin A. and Capasso F. Self-starting harmonic frequency comb generation in a quantum cascade laser. *Nature Photonics.* 2017. **11**. P. 789–792.
10. Khalatpour A., Reno J.L., Kherani N.P., and Hu Q. Unidirectional photonic wire laser. *Nature Photonics*. 2017. **11**. P. 555–559.
11. Faist J., Villares G., Scalari G., Rösch M., Bonzon C., Hugi A., Beck M. Quantum cascade laser frequency combs. *Nanophotonics.* 2016. **5**, No 2. P. 272–291.
12. Iotti R.C. and Rossi F. Nature of charge transport in quantum-cascade lasers. *Phys. Rev. Lett*. 2001. **87**. P. 146603-1–146603-4.
13. Wacker A. Gain in quantum cascade lasers and superlattices: A quantum transport theory. *Phys. Rev. B*. 2002. **66**. P. 085326.
14. Lee S-C. and Wacker A. Nonequilibrium Green's function theory for transport and gain properties of quantum cascade structures. *Phys. Rev. B*. 2002. **66**, No 24. P. 245314.

15. Donovan K., Harrison P., and Kelsall R.W. Self-consistent solutions to the intersubband rate equations in quantum cascade lasers: Analysis of a GaAs/$Al_xGa_{1-x}As$ device. *J. Appl. Phys*. 2001. **89**, No 6. P. 3084–3090.
16. Schrottke L., Giehler M., Wienold M., Hey R., and Grahn H.T. Compact model for the efficient simulation of the optical gain and transport properties in THz quantum-cascade lasers. *Semicond. Sci. Technol.* 2010. **25**. P. 045025–045034.
17. Kurlov S.S., Flores Y.V., Elagin M., Semtsiv M.P., Schrottke L., Grahn H.T., Tarasov G.G., and Masselink W.T. Phenomenological scattering-rate model for the simulation of the current density and emission power in mid-infrared quantum cascade lasers. *J. Appl. Phys.* 2016. **119**. P. 134501–134506.
18. Siegman A.E. *Lasers*. University Science Books, Mill Valley, 1986.
19. Faist K., Hofstetter D., Beck M., Aellen T., Rochat M., and Blaser S. Bound-to-continuum and two-phonon resonance, quantum-cascade lasers for high duty cycle, high-temperature operation. *IEEE J. Quantum Electron*. 2002. **38**. P. 533–546.
20. Lu S.L., Schrottke L., Teitsworth S.W., Hey R., and Grahn H.T. Formation of electric-field domains in GaAs/$Al_xGa_{1-x}As$ quantum cascade laser structures. *Phys. Rev. B*. 2006. **73**. 033311 (4 p.).
21. Harrison P. *Quantum Wells, Wires and Dots: Theoretical and Computational Physics*. Wiley, Chichester, 2010.
22. Jirauschek C. and Kubis T. Modeling techniques for quantum cascade lasers. *Appl. Phys. Rev.* 2014. **1**. 011307 (P. 1–51).
23. Gradshteyn and Ryzhik's *Table of Integrals, Series, and Products.* D. Zwillinger and V. Moll (eds.). 8-th edition (Oct. 2014). P. 1184.
24. Khurgin J.B., Dikmelik Y., Liu P.Q., Hoffman A.J., Escarra M.D., Franz K.J., and Gmach C.F., Role of interface roughness in the transport and lasing characteristics of quantum-cascade lasers. *Appl.Phys. Lett.* 2009. **94**. 091101 (3 p.).

Authors and CV

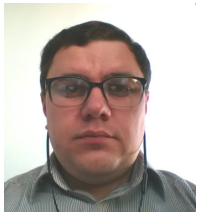

Sergii S. Kurlov received his MS degree in physics from Taras Shevchenko National University, Kyiv, Ukraine, where his studies focused on surface plasmons in Au and Al thin films for biosensors. In 2018, he defended the doctoral degree under supervision of Professor W.T. Masselink at the Humboldt University, Berlin, Germany. He investigates characterizations of InGaAs/InAlAs QCLs in the MIR and THz spectral regions. He is a member of the German Physical Society.

Mykhaylo P. Semtsiv graduated from Kyiv State University's Physics Department in 1995, having majored in solid-state optics. In 2004, he completed the doctoral degree under supervision of Professor W. T. Masselink; since then he is a scientific fellow at the Institute of Physics, Humboldt University, Berlin, with major focus on molecular beam epitaxy growth, semiconductor technology, infrared optics, quantum cascade lasers (QCLs). He is an author/coauthor in about 60 refereed journal papers and several patents on semiconductor devices.

Zoryana Y. Zhuchenko is senior researcher at V.E. Lashkaryov Institute of Semiconductor physics, NAS of Ukraine. She graduated from Drohobych Ivan Franko State Pedagogical University in 1992 with Diploma Cum Laude in Physics and Mathematics. Since 1999 Zhuchenko works at V.E. Lashkaryov Institute of Semiconductor Physics NAS of Ukraine. In 2000 she has defended PhD Dissertation in this Institute. The main directions of her investigation are physical processes in coupled nanoscale structures of different dimensionality, in part manybody excitonic effects.

Georgiy G. Tarasov defended his candidate thesis in 1979 at Institute of Semiconductors, Kyiv, Ukrain**e** with topic "Theory of non-linear optical effects in impure cubic crystals ", and then his Doctor of Sciences thesis in 1989 under the title " Non-linear polarization spectroscopy of impure cubic crystals". Since 1997 Georgiy Tarasov is Professor in Physics of Semiconductors and Insulating Crystals at ISP NAS of Ukraine. Current research interest is physics of low dimensional structures (quantum wells, dots, and wires), spin-doped multinary compounds and hetero-structures, non-linear and linear optical properties of doped crystals and glasses.

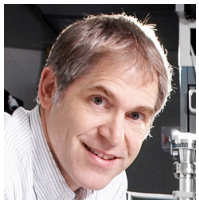

W. Ted Masselink is a Professor of Physics at the Humboldt University, Berlin, Germany. He received his PhD from the University of Illinois, Urbana, in 1986 and worked as a research physicist at the IBM T.J. Watson Research Center for 8 years. Since 1994, he has been a Full Professor in the Department of Physics, the Humboldt University, Berlin, Germany. He has authored or coauthored over 270 refereed publications, as well as a large number of conference presentations. He is a member of SPIE and APS and a senior member of the IEEE.